AN INTEGRATIVE BIOLOGY APPROACH TO QUANTIFY THE BIODISTRIBUTION OF AZIDOHOMOALANINE *IN VIVO*

Supplementary Information

Aya M. Saleh, Tyler VanDyk, Shaheryar A. Kahn,
Kathryn R. Jacobson, Sarah Calve and Tamara L. Kinzer-Ursem

Supplementary data, files, and figures for manuscript main text of the same name.

Contents

1 Code/Model Files

All model and code files can be found on our lab's GitHub repository:
https://github.itap.purdue.edu/TamaraKinzerursemGroup/ncAABiokinetics

2 System of ODEs for Aha Model

The following equations (eqs. 1-29) describe the model as diagrammed in Figure S2 using variables listed in Table S2. For clarity, equations are separated into functional components and should be evaluated in order of presentation to appropriately determine the rate of change of Aha in each compartment for each time step. For these equations, Aha is tracked in units of mass, which are converted to concentrations after the model is evaluated using appropriate tissue masses. This model was developed and parameterized with influence from previous literature [1–5].

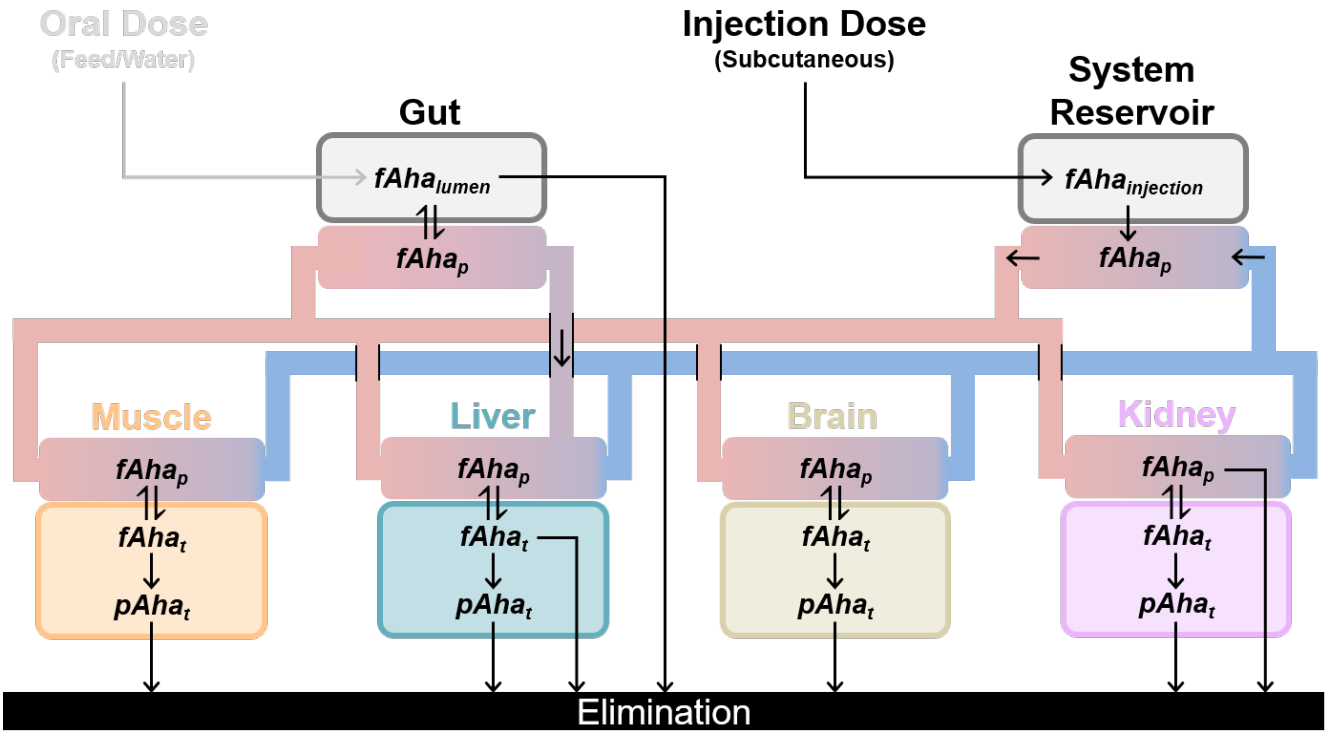

Figure S2: As seen in main text: Biodistribution of fAha via transport and exchange. Introduced at a distinct injection site, fAha is allowed to enter the circulation at a systemic venous reservoir. Driven by circulation, fAha is passed through the arterial system (red) into distinct tissue compartments where exchange occurs at tissue specific rates. Arrows indicate directional movement of fAha. Each tissue compartment consists of two sub-compartments: plasma available for surface exchange (red to blue gradient) and an intracellular volume (illustrated here as the bottom compartments: from left to right muscle, liver, brain, and kidney). A mechanism for oral dosing (via plasma exchange with the gastrointestinal lumen) is illustrated and though unused in our study is mechanistically represented in the model (eqs. 2,13,14).

Variable Definitions

Table S2: Variable definitions, see supplemental tables S3,S4,S5 for values.

kaSubcu –	subcutaneous injection site absorption rate constant
kiBrain –	fAha import rate constant from brain plasma to tissue
kiLiver –	fAha import rate constant from liver plasma to tissue
kiKidney –	fAha import rate constant from kidney plasma to tissue
kiMuscle –	fAha import rate constant from muscle plasma to tissue
keBrain –	fAha export rate constant from brain tissue to plasma
keLiver –	fAha export rate constant from liver tissue to plasma
keKidney –	fAha export rate constant from kidney tissue to plasma
keMuscle –	fAha export rate constant from muscle tissue to plasma
kiGasin –	fAha import rate constant from gut plasma to lumen
keGasin –	fAha export rate constant from gut lumen to plasma
krColon –	fAha elimination rate constant from gut lumenal excretion
krLiver –	fAha elimination rate constant from liver tissue
krKidney –	fAha elimination rate constant from urination
qbBrain –	brain tissue perfusion rate via carotid arteries
qbHepar –	liver tissue perfusion rate via the hepatic artery
qbKidney –	kidney tissue perfusion rate via renal arteries
qbMuscle –	skeletal muscle perfusion rate via peripheral arteries
qbSmint –	gut perfusion rate/liver perfusion rate via the portal vein
mbBrain –	mass of blood available for exchange with brain tissue
mbLiver –	mass of blood available for exchange with liver tissue
mbKidney –	mass of blood available for exchange with kidney tissue
mbMuscle –	mass of blood available for exchange with muscle tissue
mbSmint –	mass of blood available for exchange with gut lumen
mbSysrv –	mass of blood in the system reservoir
mbSysto –	total mass of blood in the murine body
mtBody –	mass of mouse body
mtBrain –	mass of brain tissue prior to homogenization
mtLiver –	mass of liver tissue prior to homogenization
mtKidney –	mass of kidney tissue prior to homogenization
mtMuscle –	mass of muscle tissue prior to homogenization
kdBrain –	protein degradation rate constant in brain tissue
kdLiver –	protein degradation rate constant in liver tissue
kdKidney –	protein degradation rate constant in kidney tissue
kdMuscle –	protein degradation rate constant in muscle tissue
ksBrain –	fAha incorporation rate constant in brain tissue
ksLiver –	fAha incorporation rate constant in liver tissue
ksKidney –	fAha incorporation rate constant in kidney tissue
ksMuscle –	fAha incorporation rate constant in muscle tissue
kf –	fluorescent constant, units $RFU \cdot (g\,Tissue) \cdot (\mu g\,Aha)^{-1}$

Dose Forcing Functions:

$$(fAha)_{subcu} = (fAha)_{subcu} + F(t)_{subcu} \tag{1}$$

$$(fAha)_{gasin} = (fAha)_{gasin} + F(t)_{gasin} \tag{2}$$

F(t) is typically either a cumulative step function (for injections or dietary bolus) or a continuous accumulation function (IV or watering). The model tracks the depleted pool from each dosing site ($(fAha)_{subcu}$ for injections, $(fAha)_{gasin}$ for dietary) and uses this depletion and the cumulative forcing function to determine the actual Aha mass present in each site (without changing the nomenclature) for the given time step.

Blood Flow:

$$\frac{d(fAha_p)_{muscle}}{dt} = qb_{muscle}\left(\frac{(fAha_p)_{sysrv}}{mb_{sysrv}} - \frac{(fAha_p)_{muscle}}{mb_{muscle}}\right) \tag{3}$$

$$\frac{d(fAha_p)_{liver}}{dt} = qb_{hepar}\left(\frac{(fAha_p)_{sysrv}}{mb_{sysrv}} - \frac{(fAha_p)_{liver}}{mb_{liver}}\right) \tag{4}$$

$$\frac{d(fAha_p)_{brain}}{dt} = qb_{brain}\left(\frac{(fAha_p)_{sysrv}}{mb_{sysrv}} - \frac{(fAha_p)_{brain}}{mb_{brain}}\right) \tag{5}$$

$$\frac{d(fAha_p)_{kidney}}{dt} = qb_{kidney}\left(\frac{(fAha_p)_{sysrv}}{mb_{sysrv}} - \frac{(fAha_p)_{kidney}}{mb_{kidney}}\right) \tag{6}$$

$$\frac{d(fAha_p)_{smint}}{dt} = qb_{smint}\left(\frac{(fAha_p)_{sysrv}}{mb_{sysrv}} - \frac{(fAha_p)_{smint}}{mb_{smint}}\right) \tag{7}$$

$$\frac{d(fAha_p)_{sysrv}}{dt} = -\sum_x \frac{d(fAha_p)_x}{dt} \tag{8}$$

$$\frac{d(fAha_p)_{sysrv}}{dt} \mathrel{+}= qb_{smint}\left(\frac{(fAha_p)_{liver}}{mb_{liver}} - \frac{(fAha_p)_{sysrv}}{mb_{sysrv}}\right) \tag{9}$$

$$\frac{d(fAha_p)_{liver}}{dt} \mathrel{+}= qb_{smint}\left(\frac{(fAha_p)_{smint}}{mb_{smint}} - \frac{(fAha_p)_{liver}}{mb_{liver}}\right) \tag{10}$$

Here the flow rate of Aha into each tissue from the venous reservoir is first determined (eqs. 3-7), and these inflows are inversely applied as the outflow from the system reservoir (eq. 8). Subsequently rates for the venous reservoir and liver are adjusted (eqs. 9,10) to describe the flow of blood from the system reservoir into the gut and from the gut to the liver via the portal vein. Note that the liver is fed directly from the venous reservoir via the hepatic artery (qb_{hepar}, eq. 4) and is also fed venous blood that has passed through the circulatory systems of the gut via the portal vein whose output matches the input from arteries leading to the gut (qb_{smint}, eq. 10) [4, 5].

Subcutaneous Dose Absorption:

$$\frac{d(fAha_p)_{sysrv}}{dt} \mathrel{+}= ka_{subcu}(fAha)_{subcu} \tag{11}$$

$$\frac{d(fAha)_{subcu}}{dt} = -ka_{subcu}(fAha)_{subcu} \tag{12}$$

As aforementioned, the injection site concentration of fAha is tracked as a depletion pool as it is absorbed into the system reservoir. To determine the true concentration present at each time point ($[fAha]_{subcu}$), this depletion is summed with a cumulative dosing function (eq. 1).

Oral/Dietary Gastrointestinal Dose Absorption:

$$\frac{d(fAha_p)_{smint}}{dt} \mathrel{+}= ke_{gasin}(fAha)_{gasin} - ki_{gasin}(fAha_p)_{smint} \tag{13}$$

$$\frac{d(fAha)_{gasin}}{dt} = ki_{gasin}(fAha_p)_{smint} - ke_{gasin}(fAha)_{gasin} \tag{14}$$

Even if the function $F(t)_{gasin}$ is zero for all time values, this set of equations enables GI excretion and is included in the model. If $F(t)_{gasin}$ is a dosing step function, dose absorption behaves similarly to the injection site, with the only difference being that oral dosing has a bypass mechanism directly to excretional elimination.

Tissue Exchange:

$$\frac{d(fAha_t)_{muscle}}{dt} = ki_{muscle}(fAha_p)_{muscle} - ke_{muscle}(fAha_t)_{muscle} \tag{15}$$

$$\frac{d(fAha_t)_{liver}}{dt} = ki_{liver}(fAha_p)_{liver} - ke_{liver}(fAha_t)_{liver} \tag{16}$$

$$\frac{d(fAha_t)_{brain}}{dt} = ki_{brain}(fAha_p)_{brain} - ke_{brain}(fAha_t)_{brain} \tag{17}$$

$$\frac{d(fAha_t)_{kidney}}{dt} = ki_{kidney}(fAha_p)_{kidney} - ke_{kidney}(fAha_t)_{kidney} \tag{18}$$

$$\frac{d(fAha_p)_{muscle}}{dt} -= \frac{d(fAha_t)_{muscle}}{dt} \tag{19}$$

$$\frac{d(fAha_p)_{liver}}{dt} -= \frac{d(fAha_t)_{liver}}{dt} \tag{20}$$

$$\frac{d(fAha_p)_{brain}}{dt} -= \frac{d(fAha_t)_{brain}}{dt} \tag{21}$$

$$\frac{d(fAha_p)_{kidney}}{dt} -= \frac{d(fAha_t)_{kidney}}{dt} \tag{22}$$

For tissue exchange, the import rate of fAha into the muscle is calculated for each tracked compartment (eqs. 15-18), and these rates are inverted to describe the export rate from the plasma (eqs. 19-22).

Systemic fAha Removal:

$$\frac{d(fAha_t)_{liver}}{dt} -= kr_{liver}(fAha_t)_{liver} \tag{23}$$

$$\frac{d(fAha_p)_{kidney}}{dt} -= kr_{kidney}(fAha_p)_{kidney} \tag{24}$$

$$\frac{d(fAha)_{gasin}}{dt} -= kr_{colon}(fAha)_{gasin} \tag{25}$$

Here we have represented three possible mechanisms for fAha elimination as per typical physiology and models of small molecule pharmacokinetics. The first (eq. 23 occurs within liver tissue and captures possible metabolism of an Aha utilizing native amino acid recycling machinery or elimination should the liver treat Aha as a toxin as per the functional processes of the liver [4]. The second mechanism (eq. 24 describes glomerular filtration directly from the plasma supplied to the kidneys via the renal arteries [5]. Finally, the third (eq. 25) describes excretion directly from the lumen of the gut [5].

Proteome Incorporation:

$$\frac{d(rF)_{muscle}}{dt} = kf * ks_{muscle}\frac{(fAha_t)_{muscle}}{mt_{muscle}} - kd_{muscle}(rF)_{muscle} \tag{26}$$

$$\frac{d(rF)_{liver}}{dt} = kf * ks_{liver}\frac{(fAha_t)_{liver}}{mt_{liver}} - kd_{liver}(rF)_{liver} \tag{27}$$

$$\frac{d(rF)_{brain}}{dt} = kf * ks_{brain}\frac{(fAha_t)_{brain}}{mt_{brain}} - kd_{brain}(rF)_{brain} \tag{28}$$

$$\frac{d(rF)_{kidney}}{dt} = kf * ks_{kidney}\frac{(fAha_t)_{kidney}}{mt_{kidney}} - kd_{kidney}(rF)_{kidney} \tag{29}$$

Here Aha incorporation is modeled for each tissue. As described in the main text, we make a modeling assumption that pAha is linearly proportional to rF and that the generation of pAha does not deplete fAha. We justify this assumption with both experimental findings and some back-of-the-envelop calculations. As reported in the main text, Aha is a Met analog, able to bind to methionyl tRNA synthase, albeit at a much slower rate ($k_{cat} \cdot K_m^{-1}$ Aha: 1.42E-3, Met: 5.47E-1 $\mu M^{-1} \cdot s^{-1}$) [6]. Though to our knowledge there is no reliable experimental measurements reported for the amount of Met incorporated into protein in murine tissues, Met is one of the amino acids in lower abundance. Free Met (fMet) is typically present at concentrations comparable in magnitude to the peak concentrations of Aha in measured tissues ([fMet] $\sim$ 8, 12 $\mu g \cdot g^{-1}$ in liver and kidney respectively). This yields a modeling assumption (Assumption 1) that during labeling:

$$[fAha] \approx [fMet]$$

Given the difference in the rate constant of association with methionyl tRNA synthase, at these similar concentrations, fMet likely dominates translation over fAha. Concentrations of pAha are therefore likely to be lower than pMet by a similar factor of several orders of magnitude (Assumption 2) such that within each tissue:

$$[pAha] \ll [pMet]$$

To approximate the [pMet], we can examine total cellular protein synthesis (15 $mg \cdot g^{-1} \cdot day^{-1}$, [7]), and average Met content of the proteome (3-5%, [8]), which yields a maximum pMet synthesis rate of 450-750 $\mu g \cdot g^{-1} \cdot day^{-1}$. Since fAha is only abundant for around 4 hours in our distribution model, a reasonable upper bound of [pMet] generated in that time is 125 $\mu g \cdot g^{-1}$. Without accounting for degradation, this is within an order of magnitude of the average [fMet] of our system. Therefore within this time frame we can presume (Assumption 3) that in each tissue:

$$[pMet] \approx [fMet]$$

With these assumptions in place (Assumptions 1-3), we find it possible to conclude that:

$$[pAha] \ll [pMet] \approx [fMet] \approx [fAha]$$
$$\Rightarrow [pAha] \ll [fAha]$$

Therefore, synthesis of [pAha] can be assumed dependent upon [fAha], while [fAha] can be assumed relatively independent of depletion via protein synthesis, at least in comparison to biotransport on this timescale. To further validate this assumption, we note that despite vast differences in the degree of protein labeling between tissues (for instance liver and skeletal muscles, main text figure 2E,F), there is no discernible difference in their fAha concentration profiles (main text figure 2A,B), supporting the assumption of negligible depletion of fAha by protein synthesis.

3 Parameter Table: Distribution Fit Values

Table S3: Distribution model fitting parameters. Literature from which parameters were obtained are cited. Parameters without published literature values were sourced from this study (TS) as described in methods.

Name	Best Fit Value	Units	Fitting Range	Source(s)	SE_f	$PRCC_f$
kiBrain	2.55E+1	min^{-1}	(5.0E-1, 5.0E+2)	TS	1.37E+2	1.06E-2
kiLiver	2.34E+1	min^{-1}	(5.0E-1, 5.0E+2)	TS	7.13E+1	-2.15E-1
kiKidney	6.94E+0	min^{-1}	(5.0E-1, 5.0E+2)	TS	1.66E+1	-7.27E-2
kiMuscle	6.64E+1	min^{-1}	(5.0E-1, 5.0E+2)	TS	1.57E+2	1.92E-2
keBrain	4.08E-1	min^{-1}	(1.0E-2, 1.0E+1)	TS	2.12E+0	-2.43E-1
keLiver	8.60E-1	min^{-1}	(1.0E-2, 1.0E+1)	TS	1.53E+0	-1.19E-1
keKidney	1.23E+0	min^{-1}	(1.0E-2, 1.0E+1)	TS	3.18E+0	-2.29E-1
keMuscle	3.32E-1	min^{-1}	(1.0E-2, 1.0E+1)	TS	7.65E-1	-9.64E-2
krColon	2.88E-1	min^{-1}	(3.3E-3, 3.3E-1)	[5]	5.96E+0	4.94E-2
krLiver	2.29E-1	min^{-1}	(1.0E-2, 1.0E+1)	TS	1.61E-1	-2.14E-1
krKidney	1.38E-1	min^{-1}	(1.0E-2, 1.0E+1)	[5]	2.71E+0	-1.63E-1
kiGasin	5.67E-2	min^{-1}	(1.0E-3, 1.0E+0)	[5]	4.49E-2	-1.08E-1
kaSubcu	6.18E-3	min^{-1}	(1.0E-3, 1.0E+0)	TS, [2]	9.18E-3	2.16E-2
keGasin	3.08E-2	min^{-1}	(5.0E-3, 5.0E+0)	[5]	1.88E-1	-1.08E-1
qbBrain	3.69E-1	$g \cdot min^{-1}$	(8.8E-3, 8.8E-1)	[1,2]	2.02E+0	8.03E-2
qbHepar	1.69E-1	$g \cdot min^{-1}$	(6.8E-3, 6.8E-1)	[1,2]	1.99E+0	9.34E-2
qbKidney	4.32E-1	$g \cdot min^{-1}$	(9.2E-3, 9.2E-1)	[1,2]	1.68E-1	3.38E-4
qbMuscle	4.44E-2	$g \cdot min^{-1}$	(6.8E-3, 6.8E-1)	[2,3]	7.40E-1	-6.69E-2
qbSmint	8.79E-1	$g \cdot min^{-1}$	(1.0E-2, 1.0E+0)	[1,2]	1.34E+1	1.20E-2

4 Parameter Table: Distribution Static Values

Table S4: Distribution model static parameters. All mass parameters were sourced from both the literature and experimental measurements from this study (TS) and were held constant to generate an "average" behavior according to our murine model. Compartment plasma masses were parameterized from average mass of plasma per unit mass tissue and appropriately scaled to match tissue mass utilized in this model for measurements of Aha.

Name	Model Value	Units	Physiological Range	Source(s)	PRCC
mbBrain	4.52E-3	g	(9.54E-3, 1.17E-2) g(g tissue)$^{-1}$	TS, [1,2]	6.50E-3
mbLiver	3.96E-2	g	(3.39E-2, 6.15E-2) g(g tissue)$^{-1}$	TS, [1,2]	-3.63E-3
mbKidney	3.07E-2	g	(9.65E-2, 1.37E-1) g(g tissue)$^{-1}$	TS, [1,2]	4.17E-3
mbMuscle	1.04E-3	g	(4.65E-3, 6.98E-3) g(g tissue)$^{-1}$	TS, [1,2]	3.16E-3
mbSmint	5.18E-3	g	(2.53E-4, 2.65E-4) g(g body)$^{-1}$	TS, [1,2]	5.92E-3
mbSysrv	1.09E+0	g	(4.45E-2, 6.45E-2) g(g body)$^{-1}$	TS, [1,2]	6.00E-3
mbSysto	1.17E+0	g	(4.85E-3, 6.85E-3) g(g body)$^{-1}$	TS, [1,2]	-9.99E-4
mtBody	2.00E+1	g	(1.45E+1, 2.55E+1) g	TS, [1,2]	6.03E-2
mtBrain	4.26E-1	g	(2.77E-1, 5.75E-1) g	TS, [1,2]	-5.66E-3
mtLiver	8.30E-1	g	(5.36E-1, 1.12E+0) g	TS, [1,2]	-2.51E-2
mtKidney	2.63E-1	g	(1.91E-1, 3.35E-1) g	TS, [1,2]	1.20E-3
mtMuscle	1.79E-1	g	(1.25E-1, 2.33E-1) g	TS, [1,2]	-1.34E-2

5 Parameter Table: Incorporation Fit Values

Table S5: Incorporation model fitting parameters. Since these parameters do not have published literature values, they were all sourced from this study (TS) as described in methods.

Name	Best Fit	Units	Fitting Range	Source(s)	SE_f	$PRCC_f$
kdBrain	3.54E-4	min^{-1}	(3.2E-5, 3.2E-2)	TS	1.11E-3	1.06E-2
kdLiver	8.29E-4	min^{-1}	(3.2E-5, 3.2E-2)	TS	1.80E-4	-2.15E-1
kdKidney	8.44E-4	min^{-1}	(3.2E-5, 3.2E-2)	TS	3.22E-4	-7.27E-2
kdMuscle	3.72E-4	min^{-1}	(3.2E-5, 3.2E-2)	TS	1.73E-2	1.92E-2
ksBrain	4.30E-5	min^{-1}	(2.4E-6, 2.4E-3)	TS	2.83E-5	-2.43E-1
ksLiver	3.16E-4	min^{-1}	(1.3E-5, 1.3E-2)	TS	2.49E-5	-1.19E-1
ksKidney	2.38E-4	min^{-1}	(1.2E-5, 1.2E-2)	TS	3.33E-5	-2.29E-1
ksMuscle	1.60E-6	min^{-1}	(4.2E-7, 4.2E-4)	TS	1.64E-5	-9.64E-2
*kf	1E+0	RFU(g tissue)(µg protein)$^{-1}$	*kf is included only as a scalar 1 to indicate [pAha] ∝ rF			

6 Supplementary Figure: Representative Western Blots Informing Main Text Figures 2,3

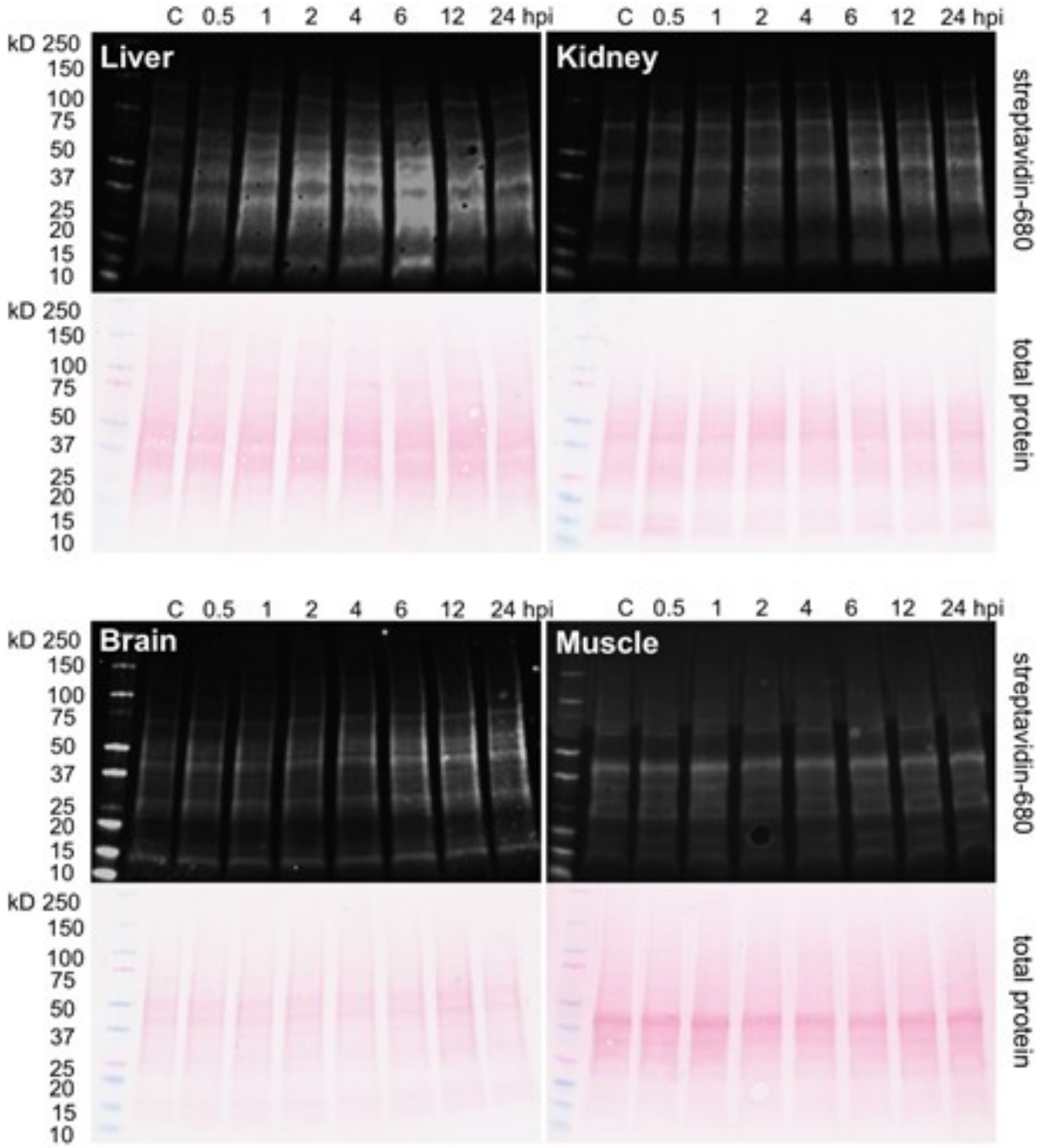

Figure S6: Representative western blots for Aha-labeled tissues at various timepoints shown in Figure 2 (top). Ponceau S staining of the western blot membrane used to confirm equal protein loading (bottom). C, control; hrd, h repeated dose; hpi, h post injection.

7 Supplementary Figure: Representative Western Blots Informing Main Text Figure 6

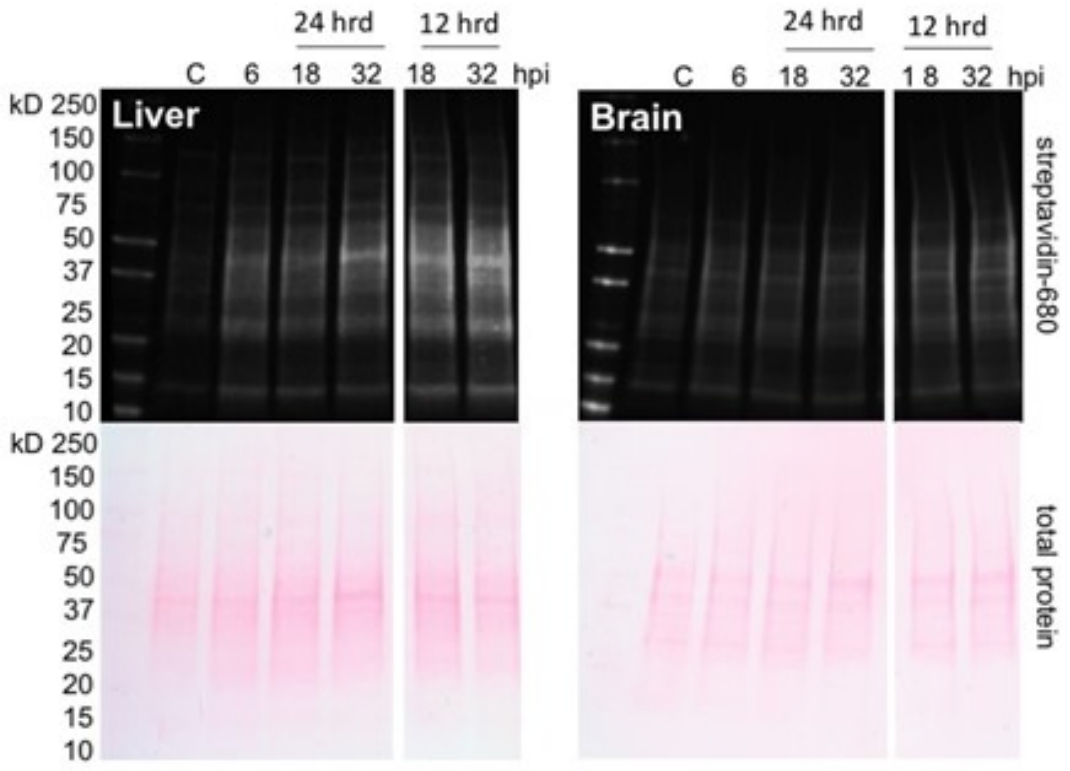

Figure S7. Representative western blots for non-injected control (C) Aha-labeled liver and brain tissues at various timepoints used for the validation of model predictive ability shown in Figure 6 (top). Ponceau S staining of the western blot membrane used to confirm equal protein loading (bottom). C, control; hrd, h repeated dose; hpi, h post injection.

References

1. Boswell, C. A. *et al.* Comparative physiology of mice and rats: Radiometric measurement of vascular parameters in rodent tissues. *Molecular Pharmaceutics* **11.** ISSN: 15438392 (5 2014).
2. Brown, G. C. Total cell protein concentration as an evolutionary constraint on the metabolic control distribution in cells. *Journal of Theoretical Biology* **153,** 195–203. ISSN: 10958541. https://pubmed.ncbi.nlm.nih.gov/1787736/ (2 Nov. 1991).
3. Streif, J. U. *et al.* In vivo assessment of absolute perfusion in the murine skeletal muscle with spin labeling MRI. *Journal of Magnetic Resonance Imaging* **17,** 147–152. ISSN: 1053-1807. http://doi.wiley.com/10.1002/jmri.10229 (1 Jan. 2003).
4. Chiang, J. in, 1770–1782 (July 2014). ISBN: 9780123864574.
5. Kirman, C. R. *et al.* Physiologically based pharmacokinetic model for rats and mice orally exposed to chromium. *Chemico-Biological Interactions* **200,** 45–64. ISSN: 00092797 (1 Oct. 2012).
6. Kiick, K., Saxon, E., Tirrell, D. & Bertozzi, C. *Incorporation of azides into recombinant proteins for chemoselective modification by the Staudinger ligation* en. in *Proceedings of the National Academy of Sciences of the United States of America* **99** (2002), 19–24.
7. Piques, M. *et al.* Ribosome and transcript copy numbers, polysome occupancy and enzyme dynamics in Arabidopsis. *Molecular Systems Biology* **5.** ISSN: 17444292. https://pubmed.ncbi.nlm.nih.gov/:19888:209/%20https://pubmed.ncbi.nlm.nih.gov/:19888:209/?dopt=Abstract (Jan. 2009).
8. Moura, A., Savageau, M. A. & Alves, R. Relative Amino Acid Composition Signatures of Organisms and Environments. *PLoS ONE* **8.** ISSN: 19326:203. /pmc/articles/PMC3808408/?report=abstract%20https://www.ncbi.nlm.nih.gov/pmc/articles/PMC3808408/ (10 Oct. 2013).